Rotating clusters in phase-lagged Kuramoto oscillators with higher-order interactions

Bhuwan Moyal,[*] Priyanka Rajwani,[*] Subhasanket Dutta, and Sarika Jalan[†]
Complex Systems Laboratory, Department of Physics, Indian Institute of Technology Indore, Khandwa Road, Simrol, Indore-453552, India

(Received 22 August 2023; revised 9 December 2023; accepted 6 February 2024; published 18 March 2024)

The effect of phase-lag in pairwise interactions has been a topic of great interest for a while. However, real-world systems often have interactions that are beyond pairwise and can be modeled using simplicial complexes. We show that the inclusion of higher-order interactions in phase-lagged coupled Kuramoto oscillators shifts the critical point at which first-order transition from a cluster synchronized state to an incoherent state takes place. Considering the polar coordinates, we obtain the rotation frequency of the clusters, which turns out to be a function of the phase-lag parameter. In turn, the phase- lag can be used as a control parameter to achieve a desired cluster frequency. Moreover, in the thermodynamic limit, by employing the Ott-Antonsen approach we derive a reduced equation for the order parameter measuring cluster synchronization and progress further through the self-consistency method to obtain a closed form of the order parameter measuring global synchronization which was lacking in the Ott-Antonsen approach.

DOI: 10.1103/PhysRevE.109.034211

I. INTRODUCTION

Synchronization of interacting units occurs in many real-world complex systems ranging from the circadian clock in the brain and neural networks to power grids, cardiac rhythms, and chemical oscillators [1]. It was the insights of Winfree that Kuramoto later utilized to model the collective phenomenon of synchronization into a more manageable form which tells us how the coupled Kuramoto oscillators progress from an incoherent to a fully coherent state through a second-order phase transition [2,3]. Later studies of the coupled Kuramoto oscillator model, with and without a phase-lag, have uncovered versatile phenomena such as global and cluster synchronization [4], partially synchronized states [5], explosive synchronization in a single layer [6], and multilayer networks [7–9], etc. Particularly, phase-frustrated coupling, which could also be perceived as time-delayed interactions, is widespread in various physical systems [10–12]. For example, in power grids the phase-lag parameter corresponds to the energy loss along the transmission lines [13]. Also, a neural network with distributed time delays can be modeled as a coupled Kuramoto model with a phase-lag parameter [14]. Sakaguchi and Kuramoto investigated the effect caused by the inclusion of a phase frustration parameter in an ensemble of oscillators and uncovered that strong coupling of oscillators can bring them together in one cluster which rotates with a nonzero frequency, deviating from the algebraic sum of the oscillator's intrinsic frequencies [15]. This contrasts with what was realized for the Kuramoto model having zero phase-lag. Further, phase-lag is found to be responsible for causing phase turbulence in self-oscillatory diffusive systems [16]. A few systems that have been modeled through Kuramoto oscillators with phase-lag parameters are seismology [17] and Josephson junctions [18,19]. Also, this model became the prototype model to investigate chimera where the nonlocally coupled oscillators voluntarily split into synchronized and incoherent populations [20].

However, all these investigations and results were largely confined to purely pairwise interactions. Recent advances have indicated that this simplistic view might not be sufficient to fully decipher the underlying mechanisms behind many real-world complex phenomena where higher-order or n-simplicial interactions exist [21,22]. In complex systems, n-simplex is formed by $n+1$ interacting nodes, for example, 2- and 3-simplex represent triangle and tetrahedron, respectively [23]. Many real-world complex systems such as the brain, scientific collaborations, and social systems have underlying higher-order interactions that are crucial for their functioning and evolution [24]. In 2019, Skardal and Arenas [25] had shown that the Kuramoto oscillators coupled through 2-simplex interactions manifest an abrupt first-order transition to desynchronization with no complementary abrupt synchronization transition. Also, in the thermodynamic limit there exists continuum desynchronization transition points arising due to changes in the initial conditions. Later Kachhvah and Jalan [26] showed that adaptive 1- and 2-simplicial interactions can lead to a first-order transition to antiphase clusters. The past few years have witnessed remarkable growth in the studies of coupled Kuramoto oscillators with higher-order interactions on single-layer networks [27–32], furthermore on multilayer networks [33,34]. Lately, Carletti *et al.* [35] showed that only some particular topological oscillators in higher-order networks exhibit global synchronization, which is not seen in any arbitrary simplicial complexes.

A recent study on a coupled Kuramoto oscillators model incorporating phase-lag parameter α in the triadic interactions along with the pairwise interactions has considered the following form of the triadic coupling, $\sin(2\theta_j - \theta_k - \theta_i - \alpha)$, where θ_i is the phase of the ith Kuramoto oscillator [36]. Here, in this article, we consider another phase reduction form of the complex Ginzberg-Landau equation for 2-simplex interactions [37], yielding the triadic coupling as

[*]These authors contributed equally to this work.
[†]sarika@iiti.ac.in

$\sin(\theta_j + \theta_k - 2\theta_i - \alpha)$. Such a form of the 2-simplex coupling in the absence of a phase-lag is known to manifest a two-cluster state that gets destroyed through an abrupt desynchronization transition as coupling strength is adiabatically decreased [25]. Here, we show that the inclusion of a phase frustration term shifts the critical desynchronization point toward the higher positive coupling strength value. That is, starting with a cluster-synchronized state, as coupling strength decreases adiabatically, desynchronization to an incoherent state occurs for larger coupling strengths than that achieved for the zero-phase-lag cases. The crucial difference between the form of the triadic interactions considered here from the form of the triadic interactions considered in Ref. [36] and other existing models having phase-lag in the pairwise interactions [15,38] is the existence of a stable two-cluster state, in contrast to a stable global synchronized state.

In the thermodynamic limit, using the Ott-Antonsen approach [39] we first derive the reduced dimensional equation for a cluster synchronization state, and then by using the self-consistency method obtain the closed forms of the order parameter corresponding to global synchronization. The challenge lies in deriving an analytical expression of the cluster frequency (Ω). Which we solved by converting the coordinates into the polar frame facilitates deriving a relation between Ω and α for higher-order interactions. Ergo, α can be used as a control parameter to regulate the rotation frequency of clusters to a desired value [40]. This is the first time, to our knowledge, a relation between the cluster frequency and phase-lag parameter is established. Further, we present the numerical simulations for finite-size networks, which show a good match with the analytical predictions performed in the thermodynamic limit.

II. MODEL

We consider a higher-order extension of the Kuramoto-Sakaguchi model with coupling taken as 2-simplex interactions,

$$\dot{\theta}_i = \omega_i + \frac{K_2}{N^2}\sum_{j=1}^{N}\sum_{k=1}^{N}\sin(\theta_j + \theta_k - 2\theta_i - \alpha), \tag{1}$$

where ω_i is the intrinsic frequency of the ith oscillator and K_2 is the 2-simplex coupling strength for N oscillators. The collective behavior of the oscillators can be analyzed using the definition of the generalized order parameter $z_q = r_q e^{\iota\psi_q} = \frac{1}{N}\sum_{j=1}^{N} e^{q\iota\theta_j}$ for $q = 1, 2$, where r_1 and r_2 measure the magnitude of global and two-cluster synchronization, respectively. Two-cluster synchronization refers to the state in which oscillators get locked in two clusters rather than one single cluster. Further, here $r_1 = r_2 = 0$ indicates that oscillators are uniformly distributed in a circle of unit radius referred to as an incoherent state, whereas $r_1 = r_2 = 1$ implies the global synchronization in which all oscillators are locked in a single cluster. Another case of $r_1 = 0$ and $r_2 = 1$ indicates antiphase two-cluster synchronization. The mean phase ψ_q can be calculated as

$$\psi_q = \arctan\left(\frac{\sum_{j=1}^{N}\sin(q\theta_j)}{\sum_{j=1}^{N}\cos(q\theta_j)}\right). \tag{2}$$

III. MEAN-FIELD EQUATION AND ANALYTICAL CALCULATIONS

Order-parameter notions help us to write Eq. (1) in the mean-field form such as

$$\dot{\theta}_i = \omega_i + K_2 r_1^2 \sin(2\psi_1 - 2\theta_i - \alpha). \tag{3}$$

In the continuum limit $N \to \infty$, the state of the system can be given by density function $\rho(\theta, \omega, t)$, which describes the density of oscillators with phase between θ and $\theta + \delta\theta$ and intrinsic frequencies between ω and $\omega + \delta\omega$ at time t. Since the number of oscillators is conserved, ρ must satisfy the continuity equation

$$\frac{\partial\rho}{\partial t} = -\frac{\partial(\rho\dot{\theta})}{\partial\theta}. \tag{4}$$

Considering the frequency of each oscillator drawn from a distribution $g(\omega)$, the density function can be expanded into the Fourier series

$$\rho(\theta, \omega, t) = \frac{g(\omega)}{2\pi}\left(\sum_{n=-\infty}^{\infty}\rho_n(\omega, t)e^{\iota n\theta}\right),$$

where $\rho_n(\omega, t)$ is the nth Fourier coefficient $\rho_{-n} = \rho_n^*$ and $\rho_0(\omega, t) = 1$. We can write the density function into the sum of the symmetric and antisymmetric parts; $\rho_s(\theta + \pi, \omega, t) = \rho_s(\theta, \omega, t)$ and $\rho_a(\theta + \pi, \omega, t) = -\rho_a(\theta, \omega, t)$. The linearity property of the continuity equation suggests that individually ρ_s and ρ_a are solutions, and therefore the linear combination of both is also a solution. However, only the symmetric part allows for dimensionality reduction using Ott-Antonsen ansatz, as all the Fourier modes decay geometrically [39], i.e., $\rho_{2n}(\omega, t) = \upsilon^n(\omega, t)$ where $|\upsilon(\omega, t)| \leqslant 1$:

$$\rho_s(\theta, \omega, t) = \frac{g(\omega)}{2\pi}\left[1 + \sum_{n=1}^{\infty}\rho_{2n}(\omega, t)e^{in\theta} + \text{c.c.}\right]. \tag{5}$$

Plugging this and Eq. (3) into the continuity Eq. (4), we find that each subspace spanned by odd terms $e^{\iota n\theta}$ does not collapse into a low-dimensional manifold, whereas the subspace defined by even term $e^{2\iota n\theta}$ does, i.e., given as

$$\frac{\partial\upsilon}{\partial t} = -2\iota\upsilon\omega + K_2\left(z_1^{*2}e^{\iota\alpha} - z_1^2\upsilon^2 e^{-\iota\alpha}\right). \tag{6}$$

In the continuum limit $N \to \infty$, we have $z_2 = \int_{-\infty}^{\infty}\int_0^{2\pi}\rho_s(\theta, \omega, t)e^{2\iota\theta}d\theta d\omega$, which after inserting the Fourier series expansion of $\rho_s(\theta, \omega, t)$ reduces to $z_2 = \int_{-\infty}^{\infty} g(\omega)\upsilon^* d\omega$. Upon considering the frequency distribution $g(\omega)$ to be Lorentzian $g(\omega) = \frac{\Delta}{\pi[(\omega-\omega_0)^2+\Delta^2]}$ with mean $\omega_0 = 0$ and spread $\Delta = 1$, the complex integral z_2 can be calculated using Cauchy's residue theorem by contour integration in the negative half-plane, yielding $z_2 = \upsilon^*(\omega_0 - \iota\Delta, t)$. Further, taking the complex conjugate of Eq. (6) and substituting $\omega = \omega_0 - \iota\Delta$,

$$\frac{\partial z_2}{\partial t} = -2z_2 + K_2\left({z_1}^2 e^{-\iota\alpha} - z_1^{*2}z_2^2 e^{\iota\alpha}\right).$$

Upon employing the definition of z_2 and z_1, while separating the real and imaginary parts, Eq. (6) reduces to

$$\dot{r_2} = -2r_2 + K_2{r_1}^2\left(1 - r_2^2\right)\cos(2\psi_1 - \psi_2 - \alpha), \tag{7}$$

$$\dot{\psi_2} = K_2 r_1^2\frac{1 + r_2^2}{r_2}\sin(2\psi_1 - \psi_2 - \alpha). \tag{8}$$

Note that these equations are achieved by considering the contribution of the symmetric part (ρ_s) only, which does not accomplish an explicit relation between r_1 and K_2, Hence we proceed further with the self-consistency method.

We change the frame of reference $\theta \to \theta + \psi_1$ and enter into the rotating frame of the cluster ($\dot{\psi}_1 = \Omega$). Hence, Eq. (3) can be written as

$$\dot{\theta}_i = \omega_i - \Omega - K_2 {r_1}^2 \sin(2\theta_i + \alpha). \tag{9}$$

Note that when $\alpha = 0$, oscillators are distributed in a complex circle around the mean ψ_1 guided by the frequency distribution $g(\omega)$. Also, on changing the value of K_2 the frequency range of the locked oscillators participating in clusters remains symmetric about zero. However, for nonzero α values the effective cluster frequency for $K_2 > K_{2c}$ (i.e., the critical coupling strength where the transition occurs) will be different from the mean of intrinsic frequencies. Consequently, the synchronized clusters rotate with a common nonzero frequency Ω with the magnitude of the maximum frequency being different from that of the $\alpha = 0$ case.

Next, the whole population can be divided into two groups of the locked and drifting oscillators such as $|\frac{\omega_i - \Omega}{K_2 r_1^2}| \leqslant 1$ and $|\frac{\omega_i - \Omega}{K_2 r_1^2}| > 1$, respectively. Moreover, for the locked oscillators, the coupling form of the higher-order interactions considered in Eq. (9) renders two stable fixed points:

$$\theta^* = \frac{1}{2} \arcsin\left(\frac{\omega_i - \Omega}{K_2 r_1^2}\right) - \frac{\alpha}{2}, \qquad \theta^* + \pi. \tag{10}$$

This indicates the presence of two-cluster synchronization. Since r_1 cancels out the presence of the number of oscillators in both clusters and measures effective synchronization, to quantify two-cluster synchronization, we have defined $z_2 = r_2 e^{\iota\psi_2} = \frac{1}{N}\sum_{j=1}^{N} e^{2\iota\theta_j}$, where the value of r_2 will measure the extent of two-cluster synchronization. Further, to study the contribution of the locked oscillator the density function can be written as

$$\rho_{\text{lock}}(\theta, \omega) = \eta\delta(\theta - \theta^*) + (1 - \eta)\delta[\theta - (\theta^* + \pi)], \tag{11}$$

where η and $1 - \eta$ depict the probability of oscillators and having value θ^* and $\theta^* + \pi$, respectively. Here, $0 < \eta < 1$ signifies the fraction of locked oscillators present in the θ^* cluster. Furthermore, $z_1 = \int_{-\infty}^{\infty}\int_0^{2\pi} e^{\iota\theta}\rho_{\text{loc}}(\theta, \omega)g(\omega)d\theta d\omega$ provides the contribution from the locked oscillators, given by

$${r_1}^{\text{lock}} = (2\eta - 1)\int_{-K_2 r_1^2 + \Omega}^{K_2 r_1^2 + \Omega} e^{\iota\theta^*} g(\omega) d\omega. \tag{12}$$

Moreover, for the locked state $\dot{\theta} = 0$ [Eq. (9)], using the trigonometric identities, the above equation can be expressed as

$$\cos(\theta^* + \frac{\alpha}{2}) = \sqrt{\frac{1 + \sqrt{1 - (\frac{\omega_i - \Omega}{K_2 r_1^2})^2}}{2}},$$

$$\sin(\theta^* + \frac{\alpha}{2}) = \pm\sqrt{\frac{1 - \sqrt{1 - (\frac{\omega_i - \Omega}{K_2 r_1^2})^2}}{2}},$$

where $\theta^* = \Theta - \frac{\alpha}{2}$. The contribution of the sinusoidal term will be either positive or negative based on the limits of the integration over ω. Hence, Eq. (12) can be expressed as

$${r_1}^{\text{lock}} e^{\iota\frac{\alpha}{2}} = (2\eta - 1)\int_{-K_2 {r_1}^2 + \Omega}^{K_2 {r_1}^2 + \Omega} e^{\iota\Theta} g(\omega) d\omega.$$

By plugging the value of Θ and comparing the real and imaginary parts, the contribution from the locked oscillators gets determined as

$$\begin{aligned} {r_1}^{\text{lock}} = (2\eta - 1)\Bigg[&\cos\frac{\alpha}{2}\int_{-K_2 {r_1}^2 + \Omega}^{K_2 {r_1}^2 + \Omega} \sqrt{\frac{1 + \sqrt{1 - \left(\frac{\omega - \Omega}{K_2 {r_1}^2}\right)^2}}{2}} g(\omega) d\omega - \sin\frac{\alpha}{2}\int_{-K_2 {r_1}^2 + \Omega}^{\Omega} \sqrt{\frac{1 - \sqrt{1 - \left(\frac{\omega - \Omega}{K_2 {r_1}^2}\right)^2}}{2}} g(\omega) d\omega \\ &+ \sin\frac{\alpha}{2}\int_{\Omega}^{K_2 {r_1}^2 + \Omega} \sqrt{\frac{1 - \sqrt{1 - \left(\frac{\omega - \Omega}{K_2 {r_1}^2}\right)^2}}{2}} g(\omega) d\omega \Bigg]. \end{aligned} \tag{13}$$

In addition, to analyze the contribution of the drifting oscillators, where $|\frac{\omega_i - \Omega}{K_2 r_1^2}| > 1$,

$${r_1}^{\text{drift}} = \int_{|\frac{\omega - \Omega}{K_2 r_1^2}| > 1}\int_0^{2\pi} e^{\iota\theta}\rho_{\text{drift}}(\theta, \omega)g(\omega)d\omega d\theta, \tag{14}$$

and from Eq. (4) in the steady state, $\rho_{\text{drift}}\dot{\theta}$ should be a constant, yielding $\rho_{\text{drift}} = \frac{C}{\dot{\theta}}$, where the normalization constant is calculated as the total probability of finding the oscillators on a circle with $\int_{-\pi}^{\pi}\rho_{\text{drift}}(\theta, \omega)d(\theta) = 1$ for each ω:

$$\rho_{\text{drift}} = \frac{\sqrt{(\omega - \Omega)^2 - (K_2 {r_1}^2)^2}}{2\pi|\omega - \Omega - K_2 {r_1}^2 \sin(2\theta + \alpha)|}. \tag{15}$$

It is clear from Eq. (15), $\rho_{\text{drift}}(\theta, \omega) = \rho_{\text{drift}}(\theta + \pi, \omega)$, which yields $r_1^{\text{drift}} = 0$ [Eq. (14)], i.e., the contribution of the drifting oscillators in r_1 vanishes. Therefore $r_1 = r_1^{\text{lock}} + r_1^{\text{drift}} \approx r_1^{\text{lock}}$. Furthermore, from Eq. (7) we get the fixed-point solution of r_2 as

$$r_2 = \frac{-1 + \sqrt{1 + {K_2}^2 {r_1}^4 \cos^2\alpha}}{K_2 {r_1}^2 \cos\alpha}. \tag{16}$$

Further, to simplify the expression of the self-consistency Eq. (13), we have to determine the rotation frequency Ω. The summation in Eq. (2) can be written in terms of the contribution from the locked and drifting oscillators, $\psi_q =$

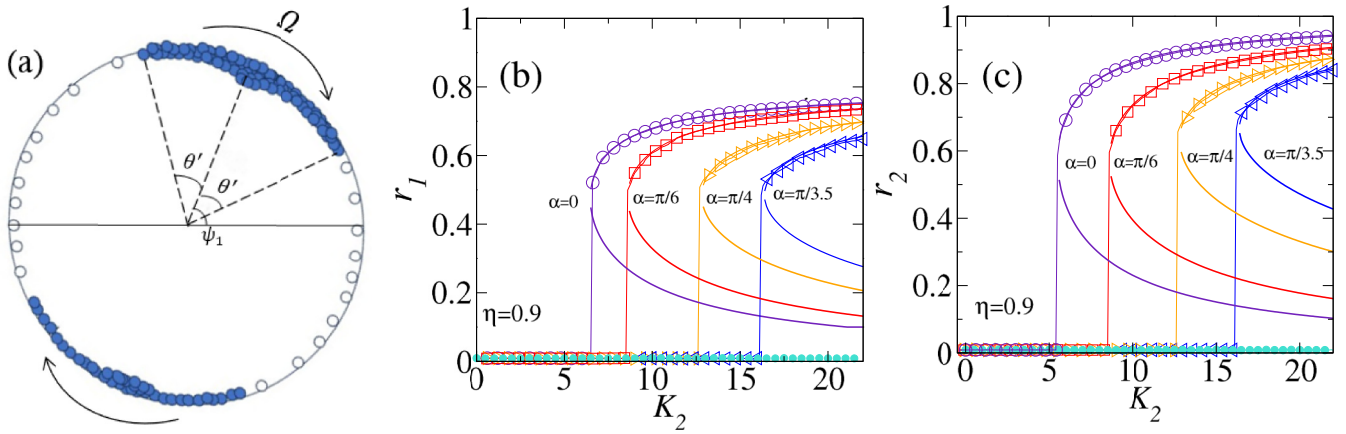

FIG. 1. (a) Schematic diagram depicting fixed points of locked (solid circle) oscillators participating with rotating clusters along with drifting (open circle) oscillators. (b) r_1 and, (c) r_2 vs K_2 for different α values depicting a shift in critical coupling strength. Here, $\alpha = 0$ (violet, open circles), $\pi/6$ (red, squares), $\pi/4$ (orange, right triangles), and $\pi/3.5$ (blue, left triangles). These results are obtained numerically by simulating Eq. (18) adiabatically in the backward direction for $N = 10^4$ oscillators. Solid curved lines represent analytical prediction from Eqs. (13) and (16) using Ω values from Eq. (17). Solid circles correspond to numerical simulation in the forward direction.

$\arctan(\frac{\langle\sin(q\theta)\rangle_{\text{lock}}+\langle\sin(q\theta)\rangle_{\text{drift}}}{\langle\cos(q\theta)\rangle_{\text{lock}}+\langle\cos(q\theta)\rangle_{\text{drift}}})$. Oscillators lie in two clusters having π phase difference [Eq. (10)]. It is straightforward now to see that contributions from the drifting oscillators cancel out due to the symmetric density distribution [Eq. (15)], as depicted in Fig. 1(a). To calculate the arguments of ψ_2, we first expand the $\langle\sin(q\theta)\rangle_{\text{lock}}$ term in one cluster which is $\eta[\sin(2\theta_1) + \sin(2\theta_2) + \cdots + \sin(2\theta_{n-1}) + \sin(2\theta_n)]$ and in another cluster, $(1-\eta)[\sin(2(\theta_1+\pi)) + \sin(2(\theta_2+\pi)) + \cdots + \sin(2(\theta_{n-1}+\pi)) + \sin(2(\theta_n+\pi))]$ and upon adding and solving we obtain,

$$\psi_2 = \arctan\left(\frac{\sin 2\theta_1 + \sin 2\theta_2 + \ldots + \sin 2\theta_{n-1} + \sin 2\theta_n}{\cos 2\theta_1 + \cos 2\theta_2 + \cdots + \cos 2\theta_{n-1} + \cos 2\theta_n}\right).$$

Then, for the locked oscillators in a cluster lying at $\psi_1 + \theta'$ there will exist another locked oscillator in the same cluster lying at $\psi_1 - \theta'$, since the intrinsic frequency distribution of oscillators is symmetric [Fig. 1(a)]. Further, simplifying the expression we get

$$\psi_2 = \arctan\left(\frac{\sin 2\psi_1[2(\cos\theta + \cos\theta' + \cdots)]}{\cos 2\psi_1[2(\cos\theta + \cos\theta' + \cdots)]}\right).$$

Thus, we obtain $\psi_2 = 2\psi_1$. This enables us to provide an important relation between the mean phase of global and cluster synchronization, which is necessary to calculate Ω as Ott-Antonsen only allows to get relation for even part of the dynamics. Next, using Eq. (8) and the above relation, we get $\dot{\psi}_1 = \Omega$, such as

$$\Omega = -\tan\alpha\sqrt{\left(1 + K_2{}^2 r_1{}^4 \cos^2\alpha\right)}. \tag{17}$$

Next, by substituting Ω from Eq. (17), the analytical values of r_1 are found by numerically integrating Eq. (13) for fixed α, K_2, and η. Note that only the locked oscillators contribute in r_1 [$r_1^{\text{drift}} = 0$, Eq. (14)]. Thereafter, we calculate r_2 from Eq. (16) by inserting values of r_1.

IV. NUMERICAL CALCULATIONS

Further, by using Eq. (17), the mean-field equation (9) reduces to

$$\dot{\theta}_i = \omega_i + \tan\alpha\sqrt{\left(1 + K_2{}^2 r_1{}^4 \cos^2\alpha\right)} - K_2 r_1{}^2 \sin(2\theta_i + \alpha). \tag{18}$$

This equation incorporating a change of the reference frame (free of ψ_1) enables us to get rid of the rotation of the cluster. We numerically simulate Eq. (18) in a rotating cluster frame free of ψ_1, instead of Eq. (3) for $N = 10^4$. The RK-4 method is used with a time step $= 0.05$, and r_1 and r_2 are obtained by averaging over 2×10^4 iterations after removing the initial transient period. We would like to note that though results from the numerical simulations of Eqs. (1) and (18) are the same as Fig. 4(a), generating simulation results for Eq. (1) is a time-consuming process.

V. RESULTS

Figure 1(a) represents the schematic distribution of oscillators in a complex unit circle. The figure illustrates that the locked oscillators are symmetrically distributed on a unit circle following the nature of the Lorentz distribution of the intrinsic frequency. There exist two antiphase clusters with the locked oscillators density being η and $1-\eta$, respectively rotating with a common angular frequency Ω. Figures 1(b) and 1(c) delineate r_1 and r_2 as a function of K_2 for different α values and $\eta = 0.9$. The value of r_2 remains greater than r_1, portraying two-cluster synchronization. Analytical predictions are obtained for specific values of K_2, η, and α. The solution for r_1 is derived from Eq. (13) by employing values of Ω from Eq. (17). Additionally, the solution for r_2 is determined from Eq. (16) after substituting the obtained values of r_1. There exists no forward synchronization as upon increasing K_2 the system always remains incoherent. It can be seen that with an increase in α the backward transition

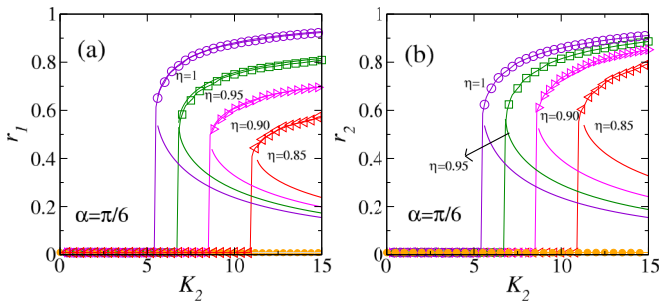

FIG. 2. Synchronization profiles depicting r_1 and r_2 as a function of K_2: (a) and (b) are for different η values. Here, $\eta = 1$ (violet, open circles), 0.95 (green, squares), 0.90 (magenta, right triangles), and 0.85 (red, left triangles). These results are obtained numerically by simulating Eq. (18) adiabatically in the backward direction. Solid lines correspond to analytical prediction obtained by Eqs. (13) and (16) using Ω values from Eq. (17). Solid circles correspond to numerical simulation in the forward direction.

point (K_{2c}) for r_1 and r_2 both shift towards the right. That is, the transition to the incoherent state occurs at a higher critical coupling value. As it happens that a nonzero α value yields a nonzero mean frequency [Eq. (17)], the intrinsic frequency range of the locked oscillators satisfying the relation $(|\frac{\omega_i-\Omega}{K_2 r_1^2}| \leqslant 1)$ no longer remains symmetric around mean 0.

Figures 2(a) and 2(b) respectively present results for r_1 and r_2 as a function of K_2 for different values of η at a fixed α value. To analyze the nature of the phase transition to synchronization, we adiabatically increase and decrease K_2, representing the forward and backward direction, respectively. In the forward direction, initially, all the oscillators are distributed uniformly between $[-\pi, \pi]$ and frequencies are drawn from a Lorentzian distribution, whereas in the backward direction, initially the oscillators are distributed into two clusters situated at diametrically opposite ends described by η. As expected, in the absence of any pairwise couplings, there exists no forward synchronization for any K_2 value, whereas the backward direction yields a first-order transition from the cluster-synchronized state to the incoherent state. With a decrease in η the critical transition point from the synchronized to the incoherent state shifts towards the right. Additionally, as η decreases, the oscillators having an initial phase lying in the locked state attempt to distribute them in diametrically opposite ends, which effectively renders fewer oscillators to contribute in r_1, due to which decreasing η leads to an increase in the transition points for both r_1 and r_2, with r_2 being greater than r_1 for $\eta < 1$, depicting cluster synchronization. In the thermodynamic limit, multistable branches exist as an infinite number of stable partially synchronized states are obtained through different arrangements of the initial conditions in two different clusters, yielding a continuum of abrupt desynchronization transitions. Moreover, we have shown the parameter space plot (η vs K_{2c}) for $\alpha = \pi/8$ and $\alpha = \pi/6$, Fig. 4(b).

In Fig. 3(a) it can be seen that for the Lorentzian distribution considered here, the symmetry breaking around the mean arising due to the inclusion of α will lead to fewer oscillators [Fig. 3(b)]. Consequently, fewer oscillators contribute to the locked state with an increase in α. Figure 3(c) plots the rotation frequency of the clusters as a function of K_2. For $\alpha = 0$ the cluster remains stationary for K_2 values, yielding $\Omega = 0$. However, for nonzero alpha values, Ω manifests a linear dependence on K_2 with an increasing slope [Eq. (17)], even for the mean intrinsic frequency being zero. This demonstrates that the phase-lag parameter regulates the rotation frequency of the synchronized clusters, which can be adjusted to a desired value by changing α. A similar phenomenon is demonstrated for pairwise interactions with phase-lag but for the global synchronization [40]. The crucial difference of the model considered here having triadic interactions from the pairwise interactions is that the former case yields two clusters, in contrast to global synchronization in the latter case.

VI. CONCLUSION AND OUTLOOK

To conclude, we have analyzed the effects of phase frustration parameters on the coupled Kuramoto oscillators on simplicial complexes. We evaluated r_1 and r_2 order parameters which measure the extent of global and two-cluster synchronization, respectively. In the absence of any pairwise

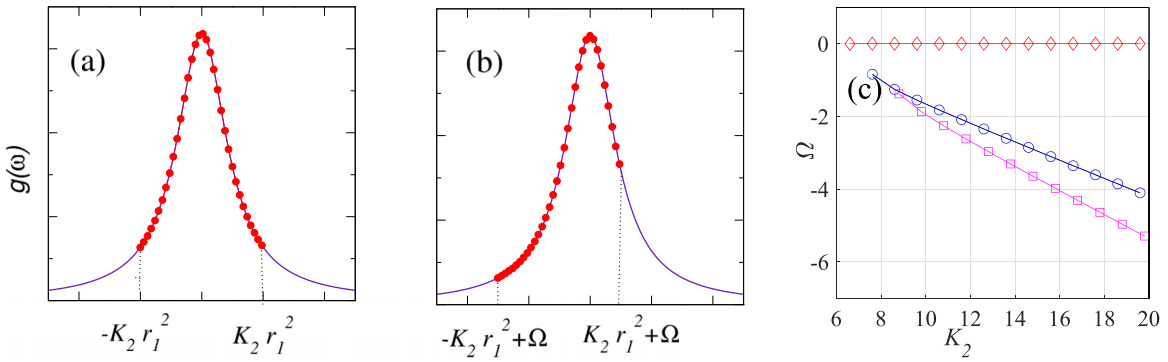

FIG. 3. Schematic diagram depicting the range of the oscillators taking part in the two-cluster state for (a) the $\alpha = 0$ case and (b) for $\alpha \neq 0$ value illustrates that oscillators taking part in the synchronized clusters may not be symmetric about mean 0. (c) K_2 vs Ω for $\eta = 0.9$ and different values of α such as 0 (red, diamonds), $\pi/8$ (blue, circles), and $\pi/6$ (magenta, squares) plotted using Eq. (17).

interactions, $r_1 = r_2 = 0$ remains at one stable state for all K_2 values. Starting with a set of initial conditions corresponding to a synchronized state, as K_2 decreases adiabatically, there exists an abrupt transition to a completely incoherent state. With an increase in the α value, this transition point for both r_1 and r_2 shifts towards the right. Further, using the Ott-Antonsen dimension reduction approach, we derived the time-dependent order parameter equations for the even part of the density function. To obtain the closed form of the asymmetric part, we proceed by the self-consistency method, which provides a relation between the order parameters (measuring global and cluster synchronization) and K_2. Additionally, to obtain the solutions for r_1 and r_2, we require an explicit expression of cluster frequency Ω, which is not achievable through the Ott-Antonsen ansatz or by the self-consistency relation, Eq. (13). We propose an analytical method for determining the expression of Ω, using a polar coordinate frame. An explicit dependence of Ω upon α indicates that α can be used as a control parameter to adjust the rotation frequency of clusters to a desired value. The analytical results are noted to be in good agreement with the numerical results. Also, dependence of the mean cluster frequency on α provides an explanation behind the origin of nonzero mean cluster frequency even for intrinsic frequency distributions having zero mean.

This model can be generalized by including a phase-lagged pairwise term along with the 2- simplex interaction for which the self-consistency analysis becomes more challenging. Moreover, this model can be extended to multilayer networks. As demonstrated by Jalan and Suman [33], multilayer networks can exhibit multiple first-order transition points instead of a single transition point to global synchronization. It will be interesting to investigate if phase-lagged higher-order interactions will lead to multiple first-transitions to cluster synchronization. Further, there have been recent attempts to analyze coupled Kuramoto oscillators with inertia on simplicial complexes [32]. An extension of the current work is to develop an analytical framework for the coupled Kuramoto model with inertia having phase-lag [41], which makes the model more generalized and suitable for wider applications.

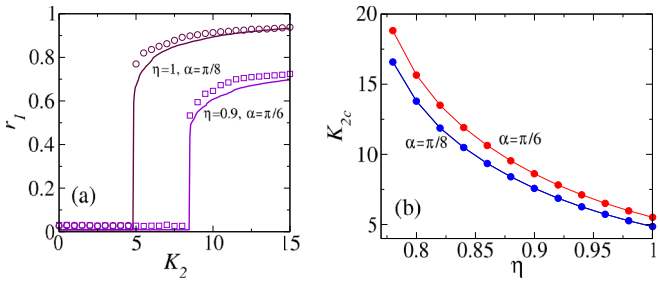

FIG. 4. (a) K_2 vs r_1. Open symbols represent direct simulation of Eq. (1) for $N = 1000$, and solid lines represent calculations from the mean-field equation (18) for $N = 10\,000$ oscillators. (b) Analytically obtained critical transition point (K_{2c}) [Eq. (13)] as a function of η for different α values.

The source code for this study is available upon request.

ACKNOWLEDGMENTS

S.J. gratefully acknowledges SERB Power Grant No. SPF/2021/000136 and useful discussions with Stefano Boccaletti under VAJRA Project No. VJR/2019/000034. P.R. is thankful to the Government of India through PMRF Grant No. PMRF/2023/2103358.

APPENDIX

K_2 vs r_1: Figure 4(a) illustrates a good match between the results obtained from direct simulation of Eq. (1) and those obtained from the mean-field equation (18), in which Ω values are calculated from Eq. (17).

Parameter space η vs K_{2c}: Figure 4(b) plots show a change in K_{2c} as a function of η for different values of phase-lag parameter α. K_{2c} decreases with an increase in η.

[1] A. Pikovsky, M. Rosenblum, and J. Kurths, *Synchronization: A Universal Concept in Nonlinear Science* (Cambridge University Press, Cambridge, England, 2003).
[2] Y. Kuramoto, Lect. Notes Phys. **39**, 420 (1975).
[3] S. H. Strogatz, Physica D **143**, 1 (2000).
[4] F. A. Rodrigues, T. K. D. Peron, P. Ji, and J. Kurths, Phys. Rep. **610**, 1 (2016).
[5] E. Omel'chenko and M. Wolfrum, Physica D **263**, 74 (2013).
[6] D. Pazó, Phys. Rev. E **72**, 046211 (2005); J. Gómez-Gardeñes, S. Gómez, A. Arenas, and Y. Moreno, Phys. Rev. Lett. **106**, 128701 (2011).
[7] X. Zhang, S. Boccaletti, S. Guan, and Z. Liu, Phys. Rev. Lett. **114**, 038701 (2015).
[8] S. Jalan, V. Rathore, A. D. Kachhvah, and A. Yadav, Phys. Rev. E **99**, 062305 (2019); S. Jalan, A. Kumar, and I. Leyva, Chaos **29**, 041102 (2019).
[9] P. Khanra, P. Kundu, C. Hens, and P. Pal, Phys. Rev. E **98**, 052315 (2018).
[10] M. Wolfrum, S. Yanchuk, and O. D'Huys, SIAM J. Appl. Dyn. Syst. **21**, 1709 (2022).
[11] S. M. Crook, G. B. Ermentrout, M. C. Vanier, and J. M. Bower, J. Comput. Neurosci. **4**, 161 (1997).
[12] C. H. Hsia, C. Y. Jung, B. Kwon, and Y. Ueda, J. Differ. Equations **268**, 7897 (2020).
[13] F. Dörfler and F. Bullo, SIAM J. Control Optim. **50**, 1616 (2012).
[14] X. Duan, E. Kang, C. Y. Liu, G.-L. Ming, and H. Song, Curr. Opin. Neurobiol. **18**, 108 (2008).
[15] H. Sakaguchi and Y. Kuramoto, Prog. Theor. Phys. **76**, 576 (1986).
[16] Y. Kuramoto, Prog. Theor. Phys. Suppl. **79**, 223 (1984).
[17] K. Vasudevan, M. Cavers, and A. Ware, Nonlin. Processes Geophys. **22**, 499 (2015).

[18] K. Wiesenfeld, P. Colet, and S. H. Strogatz, Phys. Rev. Lett. **76**, 404 (1996).
[19] G. Filatrella, N. F. Pedersen, and K. Wiesenfeld, Phys. Rev. E **61**, 2513 (2000).
[20] D. M. Abrams and S. H. Strogatz, Phys. Rev. Lett. **93**, 174102 (2004).
[21] F. Battiston, G. Cencetti, I. Iacopini, V. Latora, M. Lucas, A. Patania, J. G. Young, and G.Petri, Phys. Rep. **874**, 1 (2020).
[22] S. Boccaletti, P. De Lellis, C. I. del Genio, K. Alfaro-Bittner, R. Criado, S. Jalan, and M. Romance, Phys. Rep. **1018**, 1 (2023).
[23] F. Baccini, F. Geraci, and G. Bianconi, Phys. Rev. E **106**, 034319 (2022).
[24] I. Iacopini, G. Petri, A. Barrat, and V. Latora, Nat. Commun. **10**, 2485 (2019).
[25] P. S. Skardal and A. Arenas, Phys. Rev. Lett. **122**, 248301 (2019).
[26] A. D. Kachhvah and S. Jalan, Phys. Rev. E **105**, L062203 (2022).
[27] C. Xu and P. S. Skardal, Phys. Rev. Res. **3**, 013013 (2021).
[28] Z. Gao, D. Ghosh, H. Harrington, J. Restrepo, and D. Taylor, Chaos **33**, 040401 (2023).
[29] P. Rajwani, A. Suman, and S. Jalan, Chaos **33**, 061102 (2023).
[30] M. S. Anwar and D. Ghosh, Chaos **33**, 073111 (2023).
[31] S. Adhikari, J. G. Restrepo, and P. S. Skardal, Chaos **33**, 033116 (2023).
[32] N. G. Sabhahit, A. S. Khurd, and S. Jalan, Phys. Rev. E **109**, 024212 (2024).
[33] S. Jalan and A. Suman, Phys. Rev. E **106**, 044304 (2022).
[34] V. Rathore, A. Suman, and S. Jalan, Chaos **33**, 091105 (2023).
[35] T. Carletti, L. Giambagli, and B. Bianconi, Phys. Rev. Lett. **130**, 187401 (2023).
[36] S. Dutta, A. Mondal, P. Kundu, P. Khanra, P. Pal, and C. Hens, Phys. Rev. E **108**, 034208 (2023).
[37] I. León and D. Pazó, Phys. Rev. E **100**, 012211 (2019).
[38] E. Omel'chenko and M. Wolfrum, Phys. Rev. Lett. **109**, 164101 (2012).
[39] E. Ott and T. M. Antonsen, Chaos **18**, 037113 (2008).
[40] M. Lohe, Automatica **54**, 114 (2015).
[41] P. Jaros, S. Ghosh, D. Dudkowski, S. K. Dana, and T. Kapitaniak, Phys. Rev. E **108**, 024215 (2023).